Impact of Organic Spacers and Dimensionality on Templating of Halide Perovskites

Downloaded from: https://research.chalmers.se, 2025-12-08 23:27 UTC

Citation for the original published paper (version of record):
Fransson, E., Wiktor, J., Erhart, P. (2024). Impact of Organic Spacers and Dimensionality on Templating of Halide Perovskites. ACS Energy Letters, 9(8): 3947-3954.
http://dx.doi.org/10.1021/acsenergylett.4c01283

N.B. When citing this work, cite the original published paper.

research.chalmers.se offers the possibility of retrieving research publications produced at Chalmers University of Technology. It covers all kind of research output: articles, dissertations, conference papers, reports etc. since 2004. research.chalmers.se is administrated and maintained by Chalmers Library

(article starts on next page)

ACS Energy LETTERS

http://pubs.acs.org/journal/aelccp

Open Access

This article is licensed under CC-BY 4.0

Impact of Organic Spacers and Dimensionality on Templating of Halide Perovskites

Erik Fransson, Julia Wiktor, and Paul Erhart*

Cite This: *ACS Energy Lett.* 2024, 9, 3947−3954

Read Online

ACCESS | Metrics & More | Article Recommendations | Supporting Information

ABSTRACT: Two-dimensional (2D) halide perovskites (HPs) are promising materials for various optoelectronic applications; yet, a comprehensive understanding of their dynamics is still elusive. Here, we offer insight into the dynamics of prototypical 2D HPs based on $MAPbI_3$ as a function of linker molecule and the number of perovskite layers using atomic-scale simulations. We show that the layers closest to the linker undergo transitions that are distinct from those of the interior layers. These transitions can take place anywhere between a few tens of Kelvin degrees below and more than 100 K above the cubic−tetragonal transition of bulk $MAPbI_3$. In combination with the thickness of the perovskite layer, this enables one to template phase transitions and tune the dynamics over a wide temperature range. Our results thereby reveal the details of an important and generalizable design mechanism for tuning the properties of these materials.

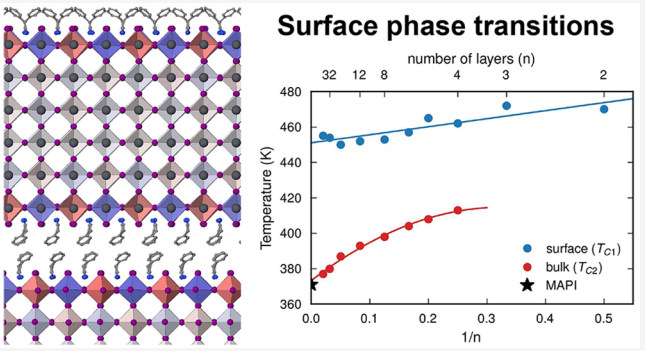

INTRODUCTION

Halide perovskites (HPs) are a promising class of materials for various applications, including, e.g., high-efficiency solar cells,[1−3] lasers[4] and light-emitting diodes.[5] The most-studied so far are the regular three-dimensional (3D) HPs with the formula AMX_3, where A is an organic or inorganic cation, M is a metal cation, such as Pb or Sn, and X is a halogen. One of the drawbacks of these compounds is that they often exhibit relatively low stability. In recent years, so-called two-dimensional (2D) HPs (also referred to as layered, quasi-2D, or Ruddlesden−Popper phases)[6] have, however, gained significant attention.[7−11] These materials are composed of inorganic perovskite layers stacked on top of each other and separated by organic cations that act as spacers (Figure 1).[12−17] They have been shown to exhibit improved stability[18−27] and distinct quantum and dielectric confinement effects,[28−30] which modulate their excitonic properties,[31−33] differentiating them from their 3D counterparts. In combination with their tunability,[34,35] this makes 2D HPs highly attractive for various optoelectronic applications.[20,35−39]

The properties of 2D HPs sensitively depend on the number and type of inorganic layers and the organic cations that connect them.[10,14,41−43] The inorganic layers are responsible for the electronic structure[44−46] and mechanical properties of the material, while the organic cations affect the interlayer spacing, as well as the overall stability and structure. Therefore, understanding the interplay of inorganic layers and organic cations is crucial for designing efficient and stable optoelectronic devices based on these materials. This is evident in the so-called "templating" approach.[47−51] This strategy relies on the fact that the organic linkers can significantly affect the phase of the inorganic framework beyond the surface layer, which can be used to improve the stability of the desired 3D

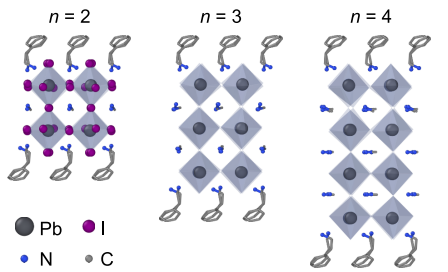

Figure 1. PEA-based 2D HP phases with the composition $PEA_2MA_{n-1}Pb_nI_{3n+1}$ for n = 2, 3, and 4 layers. For n > 2, H and I atoms are omitted for the sake of clarity. The structures were rendered using OVITO.[40]

Received: May 10, 2024
Revised: July 2, 2024
Accepted: July 5, 2024

Downloaded via CHALMERS UNIV OF TECHNOLOGY on July 30, 2024 at 08:39:26 (UTC).
See https://pubs.acs.org/sharingguidelines for options on how to legitimately share published articles.

© XXXX The Authors. Published by American Chemical Society

perovskite phases. To be able to fully exploit the potential of this approach, however, it is necessary to understand the precise mechanisms by which organic cations influence the inorganic framework.

Here, we offer comprehensive insight into how phase transitions and dynamics in 2D HPs can be steered through the choice of the organic linker molecule and the dimensionality of the material. This is accomplished through atomic-scale simulations,[52,53] based on accurate and efficient machine learning potentials (MLPs) via the neuroevolution potential (NEP) approach[53−60] trained against density functional theory (DFT) calculations[61−66] (Section S1). We first focus on the prototypical combination of the linker molecule phenylethylammonium $C_6H_5(CH_2)_2NH_3$ (PEA) with $MAPbI_3$[11,16,67,68] and identify a transition from a high-temperature structure without global octahedral tilting to a lower temperature structure with a global out-of-phase octahedral tilting pattern. The perovskite layer in direct contact with the PEA molecules (referred to as the "surface layer" below) undergoes a transition already between 450 and 470 K, while the transition in the interior of the perovskite slab occurs at a temperature that is at least 50 K lower. The combination of these two processes yields a rather broad overall transition, which approaches the transition temperature of bulk $MAPbI_3$ only for relatively thick inorganic layers comprising at least 30 or more perovskite layers. To generalize the effect of the linker molecule on the local phase transitions, we then extend the analysis to additional molecules, including phenylmethylammonium $C_6H_5(CH_2)NH_3$ (PMA), butylammonium $CH_3(CH_2)_3NH_3$ (BA) and methylammonium CH_3NH_3 (MA). We find that for bulkier molecules such as PEA and PMA, the surface layer transitions significantly above the bulk $MAPbI_3$ transition, while with the smallest molecule, MA, this transition occurs at a lower temperature. Our results thereby provide an atomic-scale understanding of how linker and dimensionality can be used to template phase behavior and dynamics in 2D HPs. Since octahedral tilting is intimately tied to the electronic structure,[69−72] our results reveal the details of an important and generalizable design mechanism for tuning the optoelectronic properties of 2D HPs.

THERMODYNAMIC PROPERTIES

We consider a series of 2D HPs assembled from inorganic PbI_6 octahedral units with MA counterions and PEA linker molecules with the chemical formula $PEA_2MA_{n-1}Pb_nI_{3n+1}$, where n is the number of *perovskite* layers in each inorganic layer (Figure 1). In the bulk limit ($n \to \infty$) one obtains $MAPbI_3$, which is one of the most widely investigated 3D HPs. We only consider systems with $n \geq 2$, since, in the single perovskite layer limit ($n = 1$), we do not observe an untilted inorganic layer, even at 600 K.

First, we analyze the potential energy, the heat capacity, and the lattice parameters during cooling simulations (Figure 2). The potential energy of $MAPbI_3$ shows a small but clear step at 370 K, corresponding to the latent heat associated with its first-order transition from a cubic $a^0a^0a^0$ phase to a tetragonal $a^0a^0c^-$ phase (Figure 2a).[60] This gives rise to a sharp peak in the heat capacity at the transition temperature (Figure 2b). Additionally, the transition can be seen as a clear change in the two in-plane lattice parameters (tilting is around the out-of-plane axis; see Figure 2c) and even the out-of-plane lattice parameter (Figure S5). The simulations yield a transition

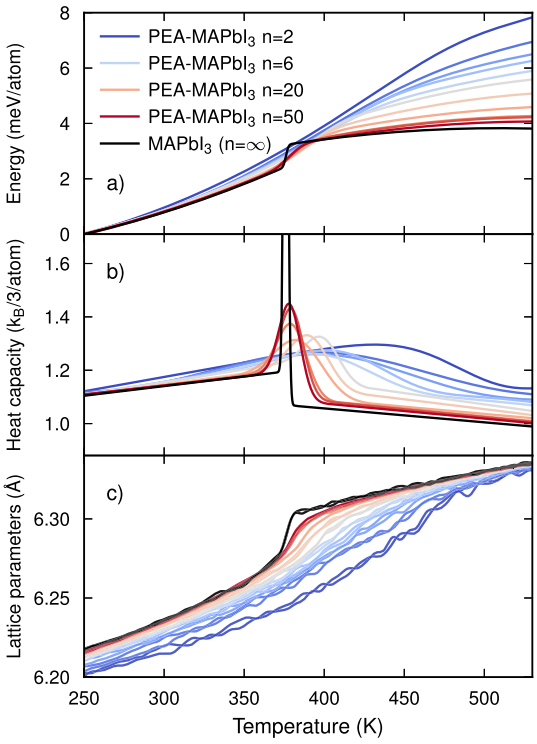

Figure 2. Thermodynamic observables as a function of temperature from cooling simulations. (a) Potential energy (with $1.5k_BT$ and arbitrary reference energy subtracted) for a series of 2D HPs with composition $PEA_2MA_{n-1}Pb_nI_{3n+1}$, which yields $MAPbI_3$ in the bulk limit ($n \to \infty$). (b) Heat capacity of the system obtained as $C_p = dE/dT$. (c) In-plane lattice parameters. For $MAPbI_3$, this corresponds to the a and b lattice parameters and the tilting in the $a^0a^0c^-$ phase occurs around the z-axis. The potential energy (and heat capacity) shown here are represented by fits to the raw data show in Figure S3.

temperature for $MAPbI_3$ of 370 K, which is ∼40 K higher than the experimental value of ∼330 K.[13,73]

Comparable transitions are observed in 2D HPs. For smaller numbers of inorganic layers (n), the transition is more gradual and occurs at higher temperatures, but it becomes more pronounced as n increases, converging toward the behavior observed in $MAPbI_3$ as n increases. This shows that the nature of the phase transition evolves from a continuous transition to a first-order transition.

OCTAHEDRAL TILTING

To obtain a more-detailed understanding of the transitions, we compute[40,74−79] (Section S1.5) the distribution over octahedral tilt angles $P(\theta)$ along the cooling simulations (Figure 3). The tilt angle distribution for a given temperature is averaged over a few snapshots corresponding to a temperature window of ∼1 K in order to improve the statistics.

For bulk $MAPbI_3$ one observes a sharp transition at 370 K from a single Gaussian peak centered around zero corresponding to a cubic phase ($a^0a^0a^0$) to a symmetric bimodal distribution indicating the transition to a structure with out-of-phase tilting ($a^0a^0c^-$; Figure 3, bottom panel).

For the 2D HPs, we can resolve the tilt angle distribution for each symmetrically distinct perovskite layer throughout the structure. This analysis reveals that the perovskite layer that is in direct contact with the PEA linker molecules (the "surface layers") undergoes a transition to a tilted structure that for, e.g.,

https://doi.org/10.1021/acsenergylett.4c01283
ACS Energy Lett. 2024, 9, 3947−3954

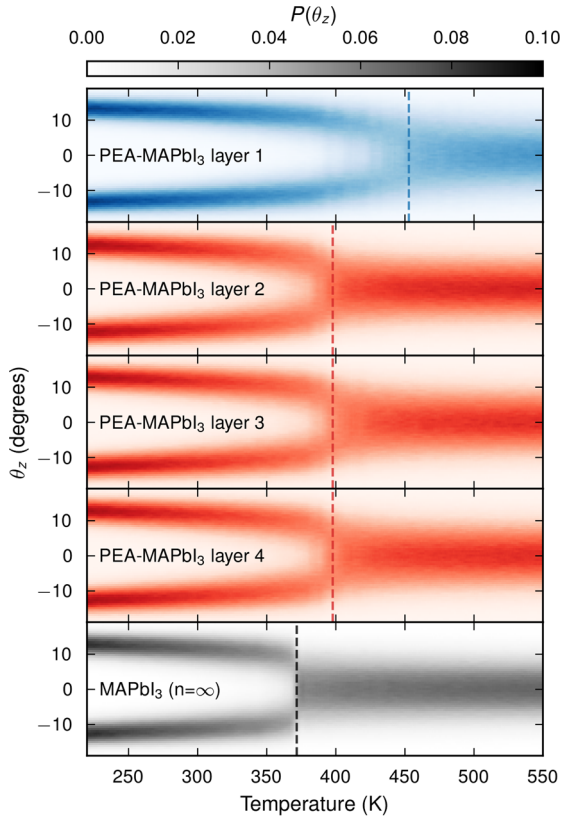

Figure 3. Distribution over the octahedral tilt angles $P(\theta_z)$ as a function of temperature for 2D HP $PEA_2MA_{n-1}Pb_nI_{3n+1}$ with n = 8, as well as the corresponding 3D HP ($MAPbI_3$). For the 2D HP, the tilt angle distribution is decomposed by a perovskite layer, where layer 1 refers to the perovskite layer closest to the organic linker molecule.

n = 8, occurs at ∼450 K (Figure 3; top panel). In contrast, the interior perovskite layers undergo a transition at a much lower temperature, i.e., closer to the bulk $MAPbI_3$ transition temperature, e.g., at ∼400 K for n = 8. It is worth noting that the transition in the surface layers has almost no impact on the tilting in the neighboring layer (layer 2 in Figure 3; also compare Figures 4b and 5b). We attribute this behavior to the octahedra rotating around the z-axis, leading to a weak correlation between neighboring octahedra in the z-direction.[74,76]

At high temperatures, for which no global tilting pattern occurs, the tilt angle distributions are unimodal and well described by Gaussians with a zero mean. The width of the distribution is, however, wider for the surface layers compared to the rest of the layers, indicating a softer free energy landscape. Furthermore, at low temperature, for which all octahedra exhibit a tilt, the surface layers show slightly larger tilt (Figure S6). Both of these observations are consistent with the surface layers exhibiting a higher transition temperature.

PHASE DIAGRAM

The spatial variation of the evolution of octahedral tilts means that the PEA-based 2D HPs internally undergo two transitions that can be observed separately in our simulations. The first one is associated with the tilting of the octahedra in the *surface* layer, while the second is related to the tilting of the *interior* layers. Extending the tilt-angle analysis for n ranging from 2 to 50 allows us to obtain the variation of the two transition temperatures with n (Figure 4). (For a brief discussion of the uncertainties in the transition temperatures, please see Section S3.) This shows that the transition in the surface layer depends only weakly on n, varying from 470 K (n = 2) to about 450 K (large-n limit). The transition in the interior, which can be identified only for $n \geq 4$, exhibits a more pronounced dependence on n starting at ∼410 K for n = 4 and converging to the bulk $MAPbI_3$ value of 370 K in the large-n limit.

The different structure of the surface layer compared to the interior resembles surface (interface) phases, also referred to as complexions.[80,81] This type of surface phases can be understood from a simplified thermodynamic viewpoint using surface and interface free energy (γ) values.[82] In this view, the observation described above suggests that the effective interface free energy between the cubic (untilted) phase and the organic linkers ($\gamma_{cub/PEA}$) is larger than the sum of the interface energy between the tetragonal (tilted) phase and the organic linkers ($\gamma_{cub/tet}$), and that between the tetragonal and cubic phases ($\gamma_{tet/PEA}$), i.e., $\gamma_{cub/PEA} > \gamma_{cub/tet} + \gamma_{tet/PEA}$.

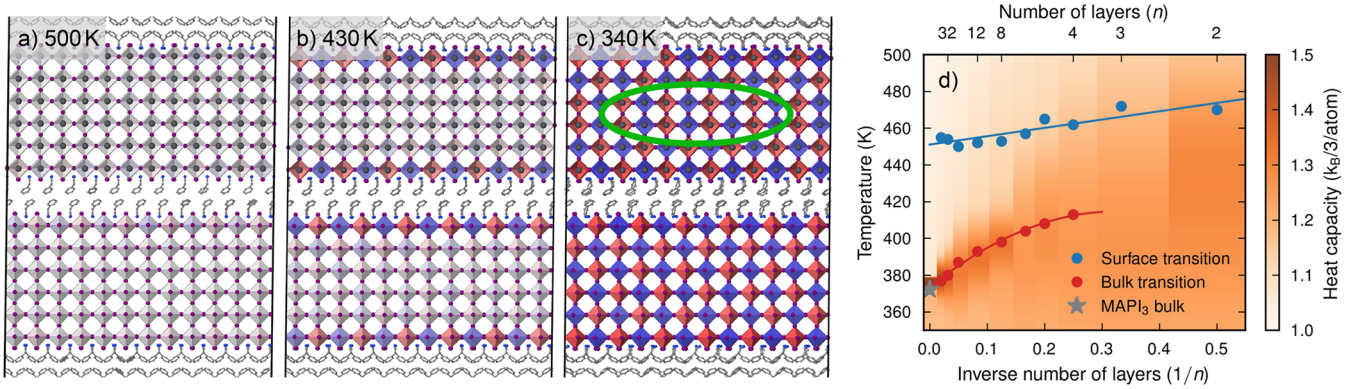

Figure 4. Time-averaged snapshots from the cooling simulations for the 2D HP $PEA_2MA_{n-1}Pb_nI_{3n+1}$ with n = 6 at (a) 500 K, (b) 430 K, and (c) 330 K visualized using OVITO.[40] Here, H atoms as well as the MA counterions inside the perovskite layers are omitted for the sake of clarity. The color coding of the octahedra indicates the rotation angle around the z-axis, θ_z, with red and blue indicating negative and positive tilting (ranging from −20° to 20°), respectively, while gray implies tilt angles close to zero. For 330 K, a stacking fault (antiphase boundary) is formed as highlighted by the green ellipsoid. (d) Transition temperatures as a function of number of layers n with the heat capacity (Figure 2), shown as a heatmap.

https://doi.org/10.1021/acsenergylett.4c01283
ACS Energy Lett. 2024, 9, 3947−3954

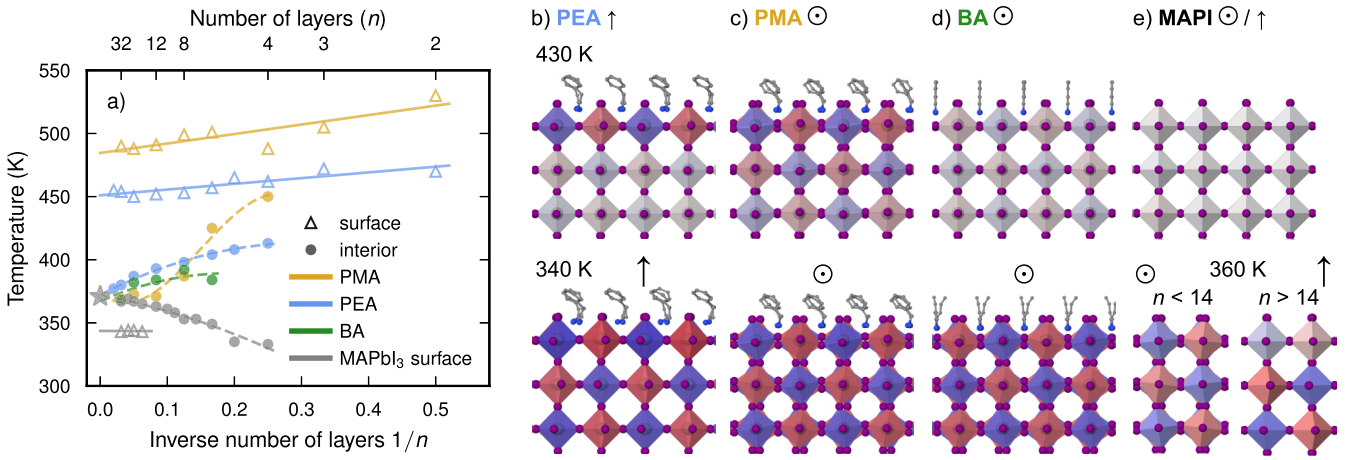

Figure 5. (a) Transition temperatures as a function of the number of layers n for (b) PEA, (c) PMA and (d) BA-based 2D HPs, as well as (e) $MAPbI_3$ surfaces. Triangles and circles indicate the transition temperatures for the surface and interior layers, respectively. The star indicates the cubic-tetragonal phase transition temperature for bulk $MAPbI_3$. (b–e) Average atomic configurations at 430 K (top) and 340/360 K (bottom). Red and blue octahedra indicate negative and positive tilt angles (ranging from −20 to 20°), respectively, whereas gray implies tilt angles close to zero. Arrows indicate the tilt axis, which is out-of-plane for PEA and $MAPbI_3$ surfaces with less than 14 layers, and in-plane for the other systems. Lines in (a) serve as a guide for the eye.

In our simulations, the tilting of the two surface layers on the opposite sides of the inorganic slab is not correlated with each other at the upper transition temperature and can thus occur by chance in-phase or out-of-phase. For the out-of-phase tilting pattern ($a^0a^0c^-$) to be commensurate with both surface layers, the latter need to tilt out-of-phase or in-phase, with respect to each other for an even and odd number of layers, n, respectively. As a result, antiphase boundaries can be expected to appear with 50% probability at nucleation time and are commonly observed in our simulations (Figure 4). In some cases, we observe such defects to anneal out already on the time scale of our simulations. Under experimental settings, one can therefore assume that such defects typically anneal out and are only present in small concentrations.

Lastly, we look at the ordering of the linker molecules. The two layers of PEA forming a single organic spacer layer are always rotated 180° around the z-axis, relative to each other (Figure 1). In addition, we observe that the different spacer layers can take on arbitrary 90 and 180° rotations around the z-axis (see e.g., Figure 4). This leads to the in-plane lattice parameters being equal (Figure 2). Reorientation and rotation of the spacer layers mainly take place during the equilibration part of the simulations, and appear to occur statistically. The orientation subsequently remains largely unaffected as temperature is reduced.

IMPACT ON THE ELECTRONIC STRUCTURE

The differences in the local structures in the interior and surface layers can be expected to affect the electronic properties of 2D perovskites. This is confirmed by an analysis of the spatial distributions of valence band maximum and conduction band minimum states using DFT calculations[83,84] (Section S4) from (MD) snapshots sampled below the lower transition (330 K), above the higher transition (530 K), and between the two transitions (430 K; compare Figure 4a–c).

The results show that at the lowest temperature (330 K), when both surface and interior layers are tilted, the valence band maximum (VBM) is localized in the middle layers, while at higher temperatures, the VBM does not preferentially localize in either type of layer. The conduction band minimum (CBM) on the other hand exhibits a strong preference to localize in the outermost layers at both the lower and intermediate temperatures, when these layers are tilted. Above the higher transition when all layers exhibit cubic symmetry, on average, the probability of finding the CBM in the middle of the perovskite slab increases. These results suggest a close relationship between the atomic scale dynamics of 2D perovskites and the electronic properties, in particular with respect to charge transport and separation, and call for further analysis in future studies.

EXTENSION TO OTHER SYSTEMS

Now that we have seen how PEA templates the phase transition in the perovskite layers, it is instructive to extend the analysis to other linker molecules. To this end, we consider 2D HPs based on PMA and BA, as well as MA-terminated surfaces, specifically, {001} slabs of $MAPbI_3$ with MAI_2 termination (Figure 5).

For PMA, the behavior is qualitatively similar to that of PEA (Figure S7), i.e., a transition of the octahedral tilting pattern occurs in the surface layer at a temperature ∼100 K higher than in the interior, albeit with a stronger dependence on the number of layers for the interior transition. Unlike the case of PEA for which we found tilting with respect to the out-of-plane axis (z), with PMA we obtain tilting around one of the in-plane axes (x or y).

For both PEA and PMA, we observe that the transition temperature for the interior increases notably with decreasing number of layers, approaching the transition temperature for the surface for the thinnest slabs considered here. This reflects the increasing relative weight of the surface layer compared to the rest of the system as n decreases. Similarly in the limit of large n, the interior transition temperature approaches that of bulk $MAPI_3$.

We also note that, in the case of PMA we observe almost no antiphase boundaries. We suggest this to be due to the stronger octahedral correlation *perpendicular* compared to *along* the rotational axis, as previously reported in bulk HPs.[74,76] This likely leads to a stronger driving force for the (re)orientation of

https://doi.org/10.1021/acsenergylett.4c01283
ACS Energy Lett. 2024, 9, 3947−3954

perovskite layers which is needed to avoid or anneal out antiphase boundaries.

By contrast, in the case of **BA**, we observe no separation in temperature between the onset of tilting at the surface and the interior. Rather, there is just one transition that for the smallest n is barely 10 to 20 K higher than the phase transition temperature for bulk $MAPbI_3$ with a very weak dependence on the number of layers. Similarly to the case of PMA, for BA the tilting occurs around one of the in-plane axes. We note that one can observe a secondary transition associated with the motion and ordering of the BA linker molecules themselves (Figure S10). At higher temperatures the BA molecules move much more freely than PEA and PMA,[44] and are on average oriented perfectly perpendicular to the perovskite layers. Below 300 K this motion is, however, frozen out and the BA molecules become significantly stiffer, in qualitative agreement with the results for $n = 1$ reported in ref 44.

For the **$MAPbI_3$ surface**, we observe two different types of behavior. For thicker slabs ($n > 14$), the topmost (surface) layer undergoes a transition at a *lower* temperature than the interior region, thus exhibiting the opposite behavior, compared to PEA and PMA. On the other hand, for thinner slabs ($n < 14$), the surface transition can no longer be separated from the transition in the interior of the slab. This can be at least partly explained by the transition temperature for the interior layers decreasing with the number of layers which causes the surface-to-interior ratio to increase. We also also observes a qualitative difference in the tilt pattern between thicker and thinner slabs as the former exhibit tilting with respect to the out-of-plane axis while for the latter tilting occurs with respect to one of the in-plane axes. This behavior suggests that the balance between surface and bulk energetics plays a key role here. While resolving the mechanism is beyond the scope of the present work it is deserving of a more in-depth analysis in future studies.

In terms of the thermodynamic viewpoint discussed above, these trends indicate that the PEA and PMA organic spacers have a favorable interaction with a tilted compared to an untilted perovskite layer, whereas for the $MAPbI_3$ surface, the opposite is true. We also note that a tilted/untilted interface along the z-direction when the tilting occurs around the x or y-axis likely has a larger interface energy compared to if the tilting occurs along the z-direction. This simple observation agrees with the fact that most cases without a surface phase transition have octahedral tilting around the x or y-direction (Figure 5).

To summarize, our analysis indicates that tilting behavior of the surface layer in 2D $MAPbI_3$-based perovskites, i.e., the softness of the rotational energy landscape of the octahedra, can be altered and controlled through the choice of the organic linker molecule. For the bulkier molecules, PEA and PMA, we find that the surface layer transitions at a considerably *higher* temperature than bulk $MAPbI_3$, whereas for the smallest molecule considered here, MA, we rather observe the surface transition to occur at a *lower* temperature than in the bulk. This leads to a transition temperature for the *interior* that decreases and increases with the number of layers for PEA/PMA and MA, respectively. For BA an intermediate behavior is observed, i.e., no separate transition for the surface layer. These results thus provide guiding principles for how both dimensionality (through the number of layers n) and chemistry (through the organic linkers) can be used to *systematically* tune the structural transitions and consequently the inorganic dynamics of the system. Both of these are directly tied to enhanced electron−phonon coupling, which is at the heart of the outstanding optoelectronic properties of these materials. The present insight is thereby of immediate interest for designing 2D HP materials and devices for specific applications and temperature ranges.

■ ASSOCIATED CONTENT

Data Availability Statement

The DFT data and NEP model generated in this study are publicly available via Zenodo at 10.5281/zenodo.11120638.

Supporting Information

The Supporting Information is available free of charge at https://pubs.acs.org/doi/10.1021/acsenergylett.4c01283.

Description of the computational methods, additional analysis of cooling simulations, transitions in additional systems, and the impact of atomic scale dynamics on the electronic structure including supporting figures (PDF)

■ AUTHOR INFORMATION

Corresponding Author

Paul Erhart − *Department of Physics, Chalmers University of Technology, SE-41296 Gothenburg, Sweden;* orcid.org/0000-0002-2516-6061; Email: erhart@chalmers.se

Authors

Erik Fransson − *Department of Physics, Chalmers University of Technology, SE-41296 Gothenburg, Sweden;* orcid.org/0000-0001-5262-3339

Julia Wiktor − *Department of Physics, Chalmers University of Technology, SE-41296 Gothenburg, Sweden;* orcid.org/0000-0003-3395-1104

Complete contact information is available at: https://pubs.acs.org/10.1021/acsenergylett.4c01283

Notes

The authors declare no competing financial interest.

■ ACKNOWLEDGMENTS

This work was supported by the Swedish Research Council (Grant Nos. 2020-04935 and 2021-05072), the Chalmers Initiative for Advancement of Neutron and Synchrotron Techniques, the Swedish Strategic Research Foundation through a Future Research Leader programme (No. FFL21-0129) and the Wallenberg Academy Fellow program (J. W.). The computations were enabled by resources provided by the National Academic Infrastructure for Supercomputing in Sweden (NAISS) at C3SE, NSC, and PDC partially funded by the Swedish Research Council through Grant Agreement Nos. 2022-06725 and 2018-05973 as well as the Berzelius resource provided by the Knut and Alice Wallenberg Foundation at NSC. We thank Göran Wahnström, Dominik Kubicki, Rasmus Lavén, Maths Karlsson, Prakriti Kayastha and Lucy Whalley for helpful discussions on 2D perovskites.

■ REFERENCES

(1) Kojima, A.; Teshima, K.; Shirai, Y.; Miyasaka, T. Organometal halide perovskites as visible-light sensitizers for photovoltaic cells. *J. Am. Chem. Soc.* **2009**, *131*, 6050−6051.

(2) Kim, H.-S.; Lee, C.-R.; Im, J.-H.; Lee, K.-B.; Moehl, T.; Marchioro, A.; Moon, S.-J.; Humphry-Baker, R.; Yum, J.-H.; Moser, J. E.; Grätzel, M.; Park, N.-G. Lead iodide perovskite sensitized all-solid-

state submicron thin film mesoscopic solar cell with efficiency exceeding 9%. *Sci. Rep.* **2012**, *2*, 1−7.
(3) Hodes, G. Perovskite-based solar cells. *Science* **2013**, *342*, 317−318.
(4) Lei, L.; Dong, Q.; Gundogdu, K.; So, F. Metal halide perovskites for laser applications. *Adv. Funct. Mater.* **2021**, *31*, 2010144.
(5) Van Le, Q.; Jang, H. W.; Kim, S. Y. Recent advances toward high-efficiency halide perovskite light-emitting diodes: review and perspective. *Small Methods* **2018**, *2*, 1700419.
(6) Akkerman, Q. A.; Manna, L. What Defines a Halide Perovskite? *ACS Energy Lett.* **2020**, *5*, 604−610.
(7) Stoumpos, C. C.; Cao, D. H.; Clark, D. J.; Young, J.; Rondinelli, J. M.; Jang, J. I.; Hupp, J. T.; Kanatzidis, M. G. Ruddlesden−Popper hybrid lead iodide perovskite 2D homologous semiconductors. *Chem. Mater.* **2016**, *28*, 2852−2867.
(8) Cao, D. H.; Stoumpos, C. C.; Farha, O. K.; Hupp, J. T.; Kanatzidis, M. G. 2D homologous perovskites as light-absorbing materials for solar cell applications. *J. Am. Chem. Soc.* **2015**, *137*, 7843−7850.
(9) Tsai, H.; et al. High-efficiency two-dimensional Ruddlesden−Popper perovskite solar cells. *Nature* **2016**, *536*, 312−316.
(10) Grancini, G.; Nazeeruddin, M. K. Dimensional tailoring of hybrid perovskites for photovoltaics. *Nat. Rev. Mater.* **2019**, *4*, 4−22.
(11) Menahem, M.; Dai, Z.; Aharon, S.; Sharma, R.; Asher, M.; Diskin-Posner, Y.; Korobko, R.; Rappe, A. M.; Yaffe, O. Strongly Anharmonic Octahedral Tilting in Two-Dimensional Hybrid Halide Perovskites. *ACS Nano* **2021**, *15*, 10153−10162.
(12) Mitzi, D. B.; Feild, C. A.; Harrison, W. T. A.; Guloy, A. M. Conducting Tin Halides with a Layered Organic-Based Perovskite Structure. *Nature* **1994**, *369*, 467−469.
(13) Stoumpos, C. C.; Malliakas, C. D.; Kanatzidis, M. G. Semiconducting Tin and Lead Iodide Perovskites with Organic Cations: Phase Transitions, High Mobilities, and Near-Infrared Photoluminescent Properties. *Inorg. Chem.* **2013**, *52*, 9019.
(14) Mao, L.; Stoumpos, C. C.; Kanatzidis, M. G. Two-Dimensional Hybrid Halide Perovskites: Principles and Promises. *J. Am. Chem. Soc.* **2019**, *141*, 1171−1190.
(15) Han, Y.; Yue, S.; Cui, B.-B. Low-Dimensional Metal Halide Perovskite Crystal Materials: Structure Strategies and Luminescence Applications. *Adv. Sci.* **2021**, *8*, 2004805.
(16) Liu, T.; Holzapfel, N. P.; Woodward, P. M. Understanding structural distortions in hybrid layered perovskites with the n = 1 Ruddlesden—Popper structure. *IUCrJ.* **2023**, *10*, 385−396.
(17) Akriti; Park, J. Y.; Zhang, S.; Dou, L. *Halide Perovskite Semiconductors*; John Wiley & Sons, Ltd., 2024; Chapter 4, pp 79−114.
(18) Smith, I. C.; Hoke, E. T.; SolisIbarra, D.; McGehee, M. D.; Karunadasa, H. I. A Layered Hybrid Perovskite Solar-Cell Absorber with Enhanced Moisture Stability. *Angew. Chem., Int. Ed.* **2014**, *53*, 11232−11235.
(19) Quan, L. N.; Yuan, M.; Comin, R.; Voznyy, O.; Beauregard, E. M.; Hoogland, S.; Buin, A.; Kirmani, A. R.; Zhao, K.; Amassian, A.; Kim, D. H.; Sargent, E. H. Ligand-Stabilized Reduced-Dimensionality Perovskites. *J. Am. Chem. Soc.* **2016**, *138*, 2649−2655.
(20) Etgar, L. The merit of perovskite's dimensionality; can this replace the 3D halide perovskite? *Energy Environ. Sci.* **2018**, *11*, 234−242.
(21) Tsai, H.; Nie, W.; Blancon, J.-C.; Stoumpos, C. C.; Soe, C. M. M.; Yoo, J.; Crochet, J.; Tretiak, S.; Even, J.; Sadhanala, A.; et al. Stable Light-Emitting Diodes Using Phase-Pure Ruddlesden-Popper Layered Perovskites. *Adv. Mater.* **2018**, *30*, 1704217.
(22) Liu, C.; Huhn, W.; Du, K.-Z.; Vazquez-Mayagoitia, A.; Dirkes, D.; You, W.; Kanai, Y.; Mitzi, D. B.; Blum, V. Tunable semiconductors: control over carrier states and excitations in layered hybrid organic-inorganic perovskites. *Phys. Rev. Lett.* **2018**, *121*, 146401.
(23) Leveillee, J.; Katan, C.; Even, J.; Ghosh, D.; Nie, W.; Mohite, A. D.; Tretiak, S.; Schleife, A.; Neukirch, A. J. Tuning electronic structure in layered hybrid perovskites with organic spacer substitution. *Nano Lett.* **2019**, *19*, 8732−8740.
(24) Mahata, A.; Meggiolaro, D.; Gregori, L.; De Angelis, F. Suppression of tin oxidation by 3D/2D perovskite interfacing. *J. Phys. Chem. C* **2021**, *125*, 10901−10908.
(25) Mosconi, E.; Alothman, A. A.; Long, R.; Kaiser, W.; De Angelis, F. Intermolecular interactions of A-site cations modulate stability of 2D metal halide perovskites. *ACS Energy Lett.* **2023**, *8*, 748−752.
(26) Park, J. Y.; Song, R.; Liang, J.; Jin, L.; Wang, K.; Li, S.; Shi, E.; Gao, Y.; Zeller, M.; Teat, S. J.; Guo, P.; Huang, L.; Zhao, Y. S.; Blum, V.; Dou, L. Thickness control of organic semiconductor-incorporated perovskites. *Nat. Chem.* **2023**, *15*, 1745−1753.
(27) Triggs, C. T.; Ross, R. D.; Mihalyi-Koch, W.; Clewett, C. F. M.; Sanders, K. M.; Guzei, I. A.; Jin, S. Spacer Cation Design Motifs for Enhanced Air Stability in Lead-Free 2D Tin Halide Perovskites. *ACS Energy Lett.* **2024**, *9*, 1835−1843.
(28) Even, J.; Pedesseau, L.; Katan, C. Understanding quantum confinement of charge carriers in layered 2D hybrid perovskites. *ChemPhysChem* **2014**, *15*, 3733−3741.
(29) Traore, B.; Pedesseau, L.; Assam, L.; Che, X.; Blancon, J.-C.; Tsai, H.; Nie, W.; Stoumpos, C. C.; Kanatzidis, M. G.; Tretiak, S.; Mohite, A. D.; Even, J.; Kepenekian, M.; Katan, C. Composite nature of layered hybrid perovskites: assessment on quantum and dielectric confinements and band alignment. *ACS Nano* **2018**, *12*, 3321−3332.
(30) Katan, C.; Mercier, N.; Even, J. Quantum and Dielectric Confinement Effects in Lower-Dimensional Hybrid Perovskite Semiconductors. *Chem. Rev.* **2019**, *119*, 3140−3192.
(31) Dyksik, M.; Duim, H.; Maude, D. K.; Baranowski, M.; Loi, M. A.; Plochocka, P. Brightening of Dark Excitons in 2D Perovskites. *Sci. Adv.* **2021**, *7*, eabk0904.
(32) Shao, Y.; Gao, W.; Yan, H.; Li, R.; Abdelwahab, I.; Chi, X.; Rogée, L.; Zhuang, L.; Fu, W.; Lau, S. P.; Yu, S. F.; Cai, Y.; Loh, K. P.; Leng, K. Unlocking surface octahedral tilt in two-dimensional Ruddlesden-Popper perovskites. *Nat. Commun.* **2022**, *13*, 138.
(33) Thompson, J. J. P.; Dyksik, M.; Peksa, P.; Posmyk, K.; Joki, A.; Perea-Causin, R.; Erhart, P.; Baranowski, M.; Loi, M. A.; Plochocka, P.; Malic, E. Phonon-bottleneck enhanced exciton emission in 2D perovskites. *Adv. Energy Mater.* **2024**, *14*, 2304343.
(34) Mahata, A.; Mosconi, E.; Meggiolaro, D.; De Angelis, F. Modulating band alignment in mixed dimensionality 3D/2D perovskites by surface termination ligand engineering. *Chem. Mater.* **2020**, *32*, 105−113.
(35) Mihalyi-Koch, W.; Folpini, G.; Roy, C. R.; Kaiser, W.; Wu, C.-S.; Sanders, K. M.; Guzei, I. A.; Wright, J. C.; De Angelis, F.; Cortecchia, D.; Petrozza, A.; Jin, S. Tuning Structure and Excitonic Properties of 2D Ruddlesden-Popper Germanium, Tin, and Lead Iodide Perovskites via Interplay between Cations. *J. Am. Chem. Soc.* **2023**, *145*, 28111−28123.
(36) Fu, W.; Liu, H.; Shi, X.; Zuo, L.; Li, X.; Jen, A. K.-Y. Tailoring the functionality of organic spacer cations for efficient and stable quasi-2D perovskite solar cells. *Adv. Funct. Mater.* **2019**, *29*, 1900221.
(37) Chen, Y.; Sun, Y.; Peng, J.; Tang, J.; Zheng, K.; Liang, Z. 2D Ruddlesden−Popper perovskites for optoelectronics. *Adv. Mater.* **2018**, *30*, 1703487.
(38) Qian, L.; Sun, Y.; Sun, M.; Fang, Z.; Li, L.; Xie, D.; Li, C.; Ding, L. 2D perovskite microsheets for high-performance photodetectors. *J. Mater. Chem. C* **2019**, *7*, 5353−5358.
(39) Yuan, S.; Fang, T.; Han, B.; Shan, Q.; Wei, C.; Zheng, X.; Li, X.; Xu, B.; Zeng, H. Ordered Phase Distribution of Quasi-2D Perovskites Controlled by a Supramolecular Approach Enables Efficient Blue Light-Emitting Diodes. *Adv. Funct. Mater.* **2024**, *34*, 2316206.
(40) Stukowski, A. Visualization and analysis of atomistic simulation data with OVITO − the Open Visualization Tool. *Modell. Simul. Mater. Sci. Eng.* **2010**, *18*, 015012.
(41) Li, X.; Hoffman, J. M.; Kanatzidis, M. G. The 2D halide perovskite rulebook: how the spacer influences everything from the structure to optoelectronic device efficiency. *Chem. Rev.* **2021**, *121*, 2230−2291.

https://doi.org/10.1021/acsenergylett.4c01283
ACS Energy Lett. 2024, 9, 3947−3954

(42) Jahanbakhshi, F.; Mladenovic, M.; Dankl, M.; Boziki, A.; Ahlawat, P.; Rothlisberger, U. Organic Spacers in 2D Perovskites: General Trends and Structure-Property Relationships from Computational Studies. *Helv. Chim. Acta* **2021**, *104*, e2000232.
(43) Kingsford, R. L.; Jackson, S. R.; Bloxham, L. C.; Bischak, C. G. Controlling Phase Transitions in Two-Dimensional Perovskites through Organic Cation Alloying. *J. Am. Chem. Soc.* **2023**, *145*, 11773−11780.
(44) Biega, R.-I.; Bokdam, M.; Herrmann, K.; Mohanraj, J.; Skrybeck, D.; Thelakkat, M.; Retsch, M.; Leppert, L. Dynamic Distortions of Quasi-2D Ruddlesden-Popper Perovskites at Elevated Temperatures: Influence on Thermal and Electronic Properties. *J. Phys. Chem. C* **2023**, *127*, 9183−9195.
(45) Ziegler, J. D.; Lin, K.-Q.; Meisinger, B.; Zhu, X.; Kober-Czerny, M.; Nayak, P. K.; Vona, C.; Taniguchi, T.; Watanabe, K.; Draxl, C.; Snaith, H. J.; Lupton, J. M.; Egger, D. A.; Chernikov, A. Excitons at the Phase Transition of 2D Hybrid Perovskites. *ACS Photonics* **2022**, *9*, 3609−3616.
(46) Krach, S.; Forero-Correa, N.; Biega, R.-I.; Reyes-Lillo, S. E.; Leppert, L. Emergence of Rashba-Dresselhaus effects in Ruddlesden−Popper halide perovskites with octahedral rotations. *J. Phys.: Condens. Matter* **2023**, *35*, 174001.
(47) Mitzi, D. B. Organic-inorganic perovskites containing trivalent metal halide layers: the templating influence of the organic cation layer. *Inorg. Chem.* **2000**, *39*, 6107−6113.
(48) Mitzi, D. B. Templating and structural engineering in organic−inorganic perovskites. *J. Chem. Soc., Dalton Trans.* **2001**, *1*, 1−12.
(49) Xu, Z.; Mitzi, D. B. SnI_4^{2-}-based hybrid perovskites templated by multiple organic cations: Combining organic functionalities through noncovalent interactions. *Chem. Mater.* **2003**, *15*, 3632−3637.
(50) Du, K.-z.; Tu, Q.; Zhang, X.; Han, Q.; Liu, J.; Zauscher, S.; Mitzi, D. B. Two-dimensional lead (II) halide-based hybrid perovskites templated by acene alkylamines: crystal structures, optical properties, and piezoelectricity. *Inorg. Chem.* **2017**, *56*, 9291−9302.
(51) Milic, J. V.; Zakeeruddin, S. M.; Grätzel, M. Layered hybrid formamidinium lead iodide perovskites: challenges and opportunities. *Acc. Chem. Res.* **2021**, *54*, 2729−2740.
(52) Fan, Z.; Chen, W.; Vierimaa, V.; Harju, A. Efficient molecular dynamics simulations with many-body potentials on graphics processing units. *Comput. Phys. Commun.* **2017**, *218*, 10−16.
(53) Fan, Z.; Wang, Y.; Ying, P.; Song, K.; Wang, J.; Wang, Y.; Zeng, Z.; Xu, K.; Lindgren, E.; Rahm, J. M.; et al. GPUMD: A package for constructing accurate machine-learned potentials and performing highly efficient atomistic simulations. *J. Chem. Phys.* **2022**, *157*, 114801.
(54) Fransson, E.; Wiktor, J.; Erhart, P. Phase Transitions in Inorganic Halide Perovskites from Machine-Learned Potentials. *J. Phys. Chem. C* **2023**, *127*, 13773−13781.
(55) Fan, Z.; Zeng, Z.; Zhang, C.; Wang, Y.; Song, K.; Dong, H.; Chen, Y.; Ala-Nissila, T. Neuroevolution machine learning potentials: Combining high accuracy and low cost in atomistic simulations and application to heat transport. *Phys. Rev. B* **2021**, *104*, 104309.
(56) Fan, Z. Improving the accuracy of the neuroevolution machine learning potential for multi-component systems. *J. Phys.: Condens. Matter* **2022**, *34*, 125902.
(57) Lindgren, E.; Rahm, M.; Fransson, E.; Eriksson, F.; Österbacka, N.; Fan, Z.; Erhart, P. calorine: A Python package for constructing and sampling neuroevolution potential models. *J. Open Source Software* **2024**, *9*, 6264.
(58) Hjorth Larsen, A.; Jørgen Mortensen, J.; Blomqvist, J.; Castelli, I. E; Christensen, R.; Dułak, M.; Friis, J.; Groves, M. N; Hammer, B.ør.; Hargus, C.; et al. The atomic simulation environmenta Python library for working with atoms. *J. Phys.: Condens. Matter* **2017**, *29*, 273002.
(59) Eriksson, F.; Fransson, E.; Erhart, P. The Hiphive Package for the Extraction of High-Order Force Constants by Machine Learning. *Adv. Theory Simul.* **2019**, *2*, 1800184.
(60) Fransson, E.; Rahm, J. M.; Wiktor, J.; Erhart, P. Revealing the Free Energy Landscape of Halide Perovskites: Metastability and Transition Characters in $CsPbBr_3$ and $MAPbI_3$. *Chem. Mater.* **2023**, *35*, 8229−8238.
(61) Kresse, G.; Hafner, J. Ab initio molecular dynamics for liquid metals. *Phys. Rev. B* **1993**, *47*, 558−561.
(62) Kresse, G.; Furthmüller, J. Efficient iterative schemes for ab initio total-energy calculations using a plane-wave basis set. *Phys. Rev. B* **1996**, *54*, 11169.
(63) Kresse, G.; Furthmüller, J. Efficiency of ab-initio total energy calculations for metals and semiconductors using a plane-wave basis set. *Comput. Mater. Sci.* **1996**, *6*, 15.
(64) Blöchl, P. E. Projector augmented-wave method. *Phys. Rev. B* **1994**, *50*, 17953−17979.
(65) Kresse, G.; Joubert, D. From ultrasoft pseudopotentials to the projector augmented-wave method. *Phys. Rev. B* **1999**, *59*, 1758−1775.
(66) Peng, H.; Yang, Z.-H.; Perdew, J. P.; Sun, J. Versatile van der Waals Density Functional Based on a Meta-Generalized Gradient Approximation. *Phys. Rev. X* **2016**, *6*, 041005.
(67) Papavassiliou, G. C.; Mousdis, G. A.; Raptopoulou, C. P.; Terzis, A. Preparation and Characterization of $[C_6H_5CH_2\ NH_3]_2PbI_4$, $[C_6H_5CH_2CH_2SC(NH_2)_2]_3PbI_5$ and $[C_{10}H_7CH_2NH_3]PbI_3$ Organic-Inorganic Hybrid Compounds. *Z. Naturforsch. B* **1999**, *54*, 1405−1409.
(68) Zuri, S.; Shapiro, A.; Kronik, L.; Lifshitz, E. Uncovering Multiple Intrinsic Chiral Phases in $(PEA)_2PbI_4$ Halide Perovskites. *J. Phys. Chem. Lett.* **2023**, *14*, 4901−4907.
(69) Filip, M. R.; Eperon, G. E.; Snaith, H. J.; Giustino, F. Steric engineering of metal-halide perovskites with tunable optical band gaps. *Nat. Commun.* **2014**, *5*, 5757.
(70) Wiktor, J.; Rothlisberger, U.; Pasquarello, A. Predictive determination of band gaps of inorganic halide perovskites. *J. Phys. Chem. Lett.* **2017**, *8*, 5507−5512.
(71) Zhao, X.-G.; Dalpian, G. M.; Wang, Z.; Zunger, A. Polymorphous nature of cubic halide perovskites. *Phys. Rev. B* **2020**, *101*, 155137.
(72) Cannelli, O.; Wiktor, J.; Colonna, N.; Leroy, L.; Puppin, M.; Bacellar, C.; Sadykov, I.; Krieg, F.; Smolentsev, G.; Kovalenko, M. V.; Pasquarello, A.; Chergui, M.; Mancini, G. F. Atomic-level description of thermal fluctuations in inorganic lead halide perovskites. *J. Phys. Chem. Lett.* **2022**, *13*, 3382−3391.
(73) Whitfield, P. S.; Herron, N.; Guise, W. E.; Page, K.; Cheng, Y. Q.; Milas, I.; Crawford, M. K. Structures, Phase Transitions and Tricritical Behavior of the Hybrid Perovskite Methyl Ammonium Lead Iodide. *Sci. Rep.* **2016**, *6*, 1−16.
(74) Wiktor, J.; Fransson, E.; Kubicki, D.; Erhart, P. Quantifying Dynamic Tilting in Halide Perovskites: Chemical Trends and Local Correlations. *Chem. Mater.* **2023**, *35*, 6737−6744.
(75) Fransson, E.; Rosander, P.; Erhart, P.; Wahnström, G. Understanding Correlations in $BaZrO_3$: Structure and Dynamics on the Nanoscale. *Chem. Mater.* **2024**, *36*, 514−523.
(76) Baldwin, W. J.; Liang, X.; Klarbring, J.; Dubajic, M.; Dell'Angelo, D.; Sutton, C.; Caddeo, C.; Stranks, S. D.; Mattoni, A.; Walsh, A.; Csányi, G. Dynamic Local Structure in Caesium Lead Iodide: Spatial Correlation and Transient Domains. *Small* **2024**, *20*, 2303565.
(77) Liang, X.; Klarbring, J.; Baldwin, W. J.; Li, Z.; Csányi, G.; Walsh, A. Structural Dynamics Descriptors for Metal Halide Perovskites. *J. Phys. Chem. C* **2023**, *127*, 19141−19151.
(78) Larsen, P. M.; Schmidt, S.; Schiøtz, J. Robust Structural Identification Via Polyhedral Template Matching. *Modell. Simul. Mater. Sci. Eng.* **2016**, *24*, 055007.
(79) Virtanen, P.; et al. SciPy 1.0: Fundamental Algorithms for Scientific Computing in Python. *Nat. Methods* **2020**, *17*, 261−272.
(80) Cantwell, P. R.; Tang, M.; Dillon, S. J.; Luo, J.; Rohrer, G. S.; Harmer, M. P. Grain boundary complexions. *Acta Mater.* **2014**, *62*, 1−48.

https://doi.org/10.1021/acsenergylett.4c01283
ACS Energy Lett. 2024, 9, 3947−3954

(81) Cantwell, P. R.; Frolov, T.; Rupert, T. J.; Krause, A. R.; Marvel, C. J.; Rohrer, G. S.; Rickman, J. M.; Harmer, M. P. Grain Boundary Complexion Transitions. *Annu. Rev. Mater. Res.* **2020**, *50*, 465−492.
(82) Johansson, S.; Wahnström, G. A computational study of thin cubic carbide films in WC/Co interfaces. *Acta Mater.* **2011**, *59*, 171−181.
(83) VandeVondele, J.; Krack, M.; Mohamed, F.; Parrinello, M.; Chassaing, T.; Hutter, J. Quickstep: Fast and accurate density functional calculations using a mixed Gaussian and plane waves approach. *Comput. Phys. Commun.* **2005**, *167*, 103−128.
(84) Kuhne, T. D.; Iannuzzi, M.; Del Ben, M.; Rybkin, V. V.; Seewald, P.; Stein, F.; Laino, T.; Khaliullin, R. Z.; Schutt, O.; Schiffmann, F.; et al. CP2K: An electronic structure and molecular dynamics software package-Quickstep: Efficient and accurate electronic structure calculations. *J. Chem. Phys.* **2020**, *152*, 194103.

https://doi.org/10.1021/acsenergylett.4c01283
ACS Energy Lett. 2024, 9, 3947−3954